

# Precision Measurement of Neutrino Oscillation Parameters with KamLAND

S. Abe,<sup>1</sup> T. Ebihara,<sup>1</sup> S. Enomoto,<sup>1</sup> K. Furuno,<sup>1</sup> Y. Gando,<sup>1</sup> K. Ichimura,<sup>1</sup> H. Ikeda,<sup>1</sup> K. Inoue,<sup>1</sup> Y. Kibe,<sup>1</sup> Y. Kishimoto,<sup>1</sup> M. Koga,<sup>1</sup> Y. Konno,<sup>1</sup> A. Kozlov,<sup>1</sup> Y. Minekawa,<sup>1</sup> T. Mitsui,<sup>1</sup> K. Nakajima,<sup>1,\*</sup> K. Nakajima,<sup>1</sup> K. Nakamura,<sup>1</sup> M. Nakamura,<sup>1</sup> K. Owada,<sup>1</sup> I. Shimizu,<sup>1</sup> J. Shirai,<sup>1</sup> F. Suekane,<sup>1</sup> A. Suzuki,<sup>1</sup> Y. Takemoto,<sup>1</sup> K. Tamae,<sup>1</sup> A. Terashima,<sup>1</sup> H. Watanabe,<sup>1</sup> E. Yonezawa,<sup>1</sup> S. Yoshida,<sup>1</sup> J. Busenitz,<sup>2</sup> T. Classen,<sup>2</sup> C. Grant,<sup>2</sup> G. Keefer,<sup>2</sup> D.S. Leonard,<sup>2</sup> D. McKee,<sup>2</sup> A. Piepke,<sup>2</sup> M.P. Decowski,<sup>3</sup> J.A. Detwiler,<sup>3</sup> S.J. Freedman,<sup>3</sup> B.K. Fujikawa,<sup>3</sup> F. Gray,<sup>3,†</sup> E. Guardincerri,<sup>3</sup> L. Hsu,<sup>3,‡</sup> R. Kadel,<sup>3</sup> C. Lendvai,<sup>3</sup> K.-B. Luk,<sup>3</sup> H. Murayama,<sup>3</sup> T. O'Donnell,<sup>3</sup> H.M. Steiner,<sup>3</sup> L.A. Winslow,<sup>3</sup> D.A. Dwyer,<sup>4</sup> C. Jillings,<sup>4,§</sup> C. Mauger,<sup>4</sup> R.D. McKeown,<sup>4</sup> P. Vogel,<sup>4</sup> C. Zhang,<sup>4</sup> B.E. Berger,<sup>5</sup> C.E. Lane,<sup>6</sup> J. Maricic,<sup>6</sup> T. Miletic,<sup>6</sup> M. Batygov,<sup>7</sup> J.G. Learned,<sup>7</sup> S. Matsuno,<sup>7</sup> S. Pakvasa,<sup>7</sup> J. Foster,<sup>8</sup> G.A. Horton-Smith,<sup>8</sup> A. Tang,<sup>8</sup> S. Dazeley,<sup>9,¶</sup> K.E. Downum,<sup>10</sup> G. Gratta,<sup>10</sup> K. Tolich,<sup>10</sup> W. Bugg,<sup>11</sup> Y. Efremenko,<sup>11</sup> Y. Kamyshev,<sup>11</sup> O. Perevozchikov,<sup>11</sup> H.J. Karwowski,<sup>12</sup> D.M. Markoff,<sup>12</sup> W. Tornow,<sup>12</sup> K.M. Heeger,<sup>13</sup> F. Piquemal,<sup>14</sup> and J.-S. Ricol<sup>14</sup>

(The KamLAND Collaboration)

<sup>1</sup>Research Center for Neutrino Science, Tohoku University, Sendai 980-8578, Japan

<sup>2</sup>Department of Physics and Astronomy, University of Alabama, Tuscaloosa, Alabama 35487, USA

<sup>3</sup>Physics Department, University of California, Berkeley and

Lawrence Berkeley National Laboratory, Berkeley, California 94720, USA

<sup>4</sup>W. K. Kellogg Radiation Laboratory, California Institute of Technology, Pasadena, California 91125, USA

<sup>5</sup>Department of Physics, Colorado State University, Fort Collins, Colorado 80523, USA

<sup>6</sup>Physics Department, Drexel University, Philadelphia, Pennsylvania 19104, USA

<sup>7</sup>Department of Physics and Astronomy, University of Hawaii at Manoa, Honolulu, Hawaii 96822, USA

<sup>8</sup>Department of Physics, Kansas State University, Manhattan, Kansas 66506, USA

<sup>9</sup>Department of Physics and Astronomy, Louisiana State University, Baton Rouge, Louisiana 70803, USA

<sup>10</sup>Physics Department, Stanford University, Stanford, California 94305, USA

<sup>11</sup>Department of Physics and Astronomy, University of Tennessee, Knoxville, Tennessee 37996, USA

<sup>12</sup>Triangle Universities Nuclear Laboratory, Durham, North Carolina 27708, USA and

Physics Departments at Duke University, North Carolina Central University, and the University of North Carolina at Chapel Hill

<sup>13</sup>Department of Physics, University of Wisconsin, Madison, Wisconsin 53706, USA

<sup>14</sup>CEN Bordeaux-Gradignan, IN2P3-CNRS and University Bordeaux I, F-33175 Gradignan Cedex, France

(Dated: February 6, 2020)

The KamLAND experiment has determined a precise value for the neutrino oscillation parameter  $\Delta m_{21}^2$  and stringent constraints on  $\theta_{12}$ . The exposure to nuclear reactor anti-neutrinos is increased almost fourfold over previous results to  $2.44 \times 10^{32}$  proton-yr due to longer livetime and an enlarged fiducial volume. An undistorted reactor  $\bar{\nu}_e$  energy spectrum is now rejected at  $>5\sigma$ . Extending the analysis down to the inverse beta decay energy threshold, and incorporating geo-neutrinos, gives a best-fit at  $\Delta m_{21}^2 = 7.58_{-0.13}^{+0.14}(\text{stat})_{-0.15}^{+0.15}(\text{syst}) \times 10^{-5} \text{ eV}^2$  and  $\tan^2 \theta_{12} = 0.56_{-0.07}^{+0.10}(\text{stat})_{-0.06}^{+0.10}(\text{syst})$ . Local  $\Delta\chi^2$ -minima at higher and lower  $\Delta m_{21}^2$  are disfavored at  $>4\sigma$ . Combining with solar neutrino data, we obtain  $\Delta m_{21}^2 = 7.59_{-0.21}^{+0.21} \times 10^{-5} \text{ eV}^2$  and  $\tan^2 \theta_{12} = 0.47_{-0.05}^{+0.06}$ .

PACS numbers: 14.60.Pq, 26.65.+t, 28.50.Hw, 91.35.-x

Experiments studying atmospheric, solar, reactor and accelerator neutrinos provide compelling evidence for neutrino mass and oscillation. The Kamioka Liquid scintillator Anti-Neutrino Detector (KamLAND) investigates neutrino oscillation parameters by observing electron anti-neutrinos ( $\bar{\nu}_e$ ) emitted from distant nuclear reactors. Previously, KamLAND announced the first evidence of  $\bar{\nu}_e$  disappearance [1], followed by direct evidence for neutrino oscillation by observing distortion of the reactor  $\bar{\nu}_e$  energy spectrum [2]. More recently, KamLAND showed the first indication of geologically produced anti-neutrinos (geo-neutrinos) from radioactive decay in the Earth [3], possibly a unique tool for geology.

This Letter presents a precise measurement of  $\Delta m_{21}^2$  and new constraints on  $\theta_{12}$  based on data collected from March 9, 2002 to May 12, 2007, including data periods used in earlier reports [1, 2]. We have enlarged the fiducial volume

diameter from 5.5 m to 6 m and collected significantly more data; the total exposure is  $2.44 \times 10^{32}$  proton-yr (2881 ton-yr). We have expanded the analysis to the full reactor  $\bar{\nu}_e$  energy spectrum and reduced the systematic uncertainties in the number of target protons and the background. We now observe almost two complete oscillation cycles in the  $\bar{\nu}_e$  spectrum and extract more precise values of the oscillation parameters. The confidence level for geo-neutrino detection is modestly improved.

KamLAND is situated at the site of the former Kamiokande experiment at a depth of  $\sim 2700$  m water equivalent. The heart of the detector is 1 kton of highly purified liquid scintillator (LS) enclosed in an EVOH/nylon balloon suspended in purified mineral oil. The LS consists of 80% dodecane, 20% pseudocumene and  $1.36 \pm 0.03$  g/l of PPO [19] as a fluor. The anti-neutrino detector is contained inside an 18-m-diameter stainless steel sphere. An array of 1879 50-cm-diameter pho-

tomultiplier tubes (PMTs) is mounted on the inner surface of the sphere. A subset of 554 PMTs, referred to as “20-inch tubes”, are reused from the Kamiokande experiment, while the remaining 1325 PMTs are a faster version masked to 17 inches. A 3.2-kton cylindrical water-Cherenkov outer detector (OD), surrounding the containment sphere, provides shielding and operates as an active cosmic-ray veto detector.

Electron anti-neutrinos are detected via inverse  $\beta$ -decay,  $\bar{\nu}_e + p \rightarrow e^+ + n$ , with a 1.8 MeV threshold. The prompt scintillation light from the  $e^+$  gives a measure of the incident  $\bar{\nu}_e$  energy,  $E_{\bar{\nu}_e} \simeq E_p + \bar{E}_n + 0.8 \text{ MeV}$ , where  $E_p$  is the prompt event energy including the positron kinetic and annihilation energy, and  $\bar{E}_n$  is the average neutron recoil energy,  $O(10 \text{ keV})$ . The neutron is captured about  $200 \mu\text{s}$  mean time after the prompt event. More than 99% capture on free protons, resulting in a deuteron and a 2.2 MeV  $\gamma$  ray.

KamLAND is surrounded by 55 Japanese nuclear power reactor units, each an isotropic  $\bar{\nu}_e$  source. The reactor operation records, including thermal power generation, fuel burnup, and exchange and enrichment logs, are provided by a consortium of Japanese electric power companies. This detailed information, combined with publicly available data about the rest of the world’s reactors, is used to calculate the instantaneous fission rates using a reactor model [4]. Only four isotopes contribute significantly to the  $\bar{\nu}_e$  spectra; the ratios of the fission yields averaged over the entire data taking period are:  $^{235}\text{U} : ^{238}\text{U} : ^{239}\text{Pu} : ^{241}\text{Pu} = 0.570 : 0.078 : 0.295 : 0.057$ .  $^{90}\text{Sr}$ ,  $^{106}\text{Ru}$ , and  $^{144}\text{Ce}$ , are long-lived fission daughters and contribute low-energy neutrinos [5]. The emitted  $\bar{\nu}_e$  energy spectrum is calculated from the fission rates using the  $\bar{\nu}_e$  spectra inferred from Ref. [6], while the spectral uncertainty is evaluated from Ref. [7].

We recently commissioned an “off-axis” calibration system capable of positioning radioactive sources within 5.5 m of the center of the detector. Multiple measurements of the detector response at five distances between 2.8 m and 5.5 m indicate that the vertex reconstruction systematic effects are radius- and zenith-angle-dependent, but the vertex-position offsets are smaller than 3 cm and independent of azimuthal position. The fiducial volume (FV) is determined with 1.6% uncertainty up to 5.5 m using the off-axis calibration system. The position distribution of the  $\beta$ -decays of muon-induced  $^{12}\text{B}/^{12}\text{N}$  independently confirm this with 4.0% uncertainty by comparing the number of events inside 5.5 m to the number produced in the full LS volume. The  $^{12}\text{B}/^{12}\text{N}$  event ratio is used to establish the uncertainty between 5.5 m and 6 m, resulting in a combined 6-m-radius FV uncertainty of 1.8%.

Off-axis calibration measurements and numerous central-axis deployments of  $^{60}\text{Co}$ ,  $^{68}\text{Ge}$ ,  $^{203}\text{Hg}$ ,  $^{65}\text{Zn}$ ,  $^{137}\text{Cs}$ ,  $^{241}\text{Am}^9\text{Be}$  and  $^{210}\text{Po}^{13}\text{C}$  radioactive sources were used to establish the detector reconstruction properties. For the 17-inch and 20-inch PMTs combined, the vertex reconstruction resolution is  $\sim 12 \text{ cm}/\sqrt{E(\text{MeV})}$  and the energy resolution is  $6.5\%/\sqrt{E(\text{MeV})}$ . The scintillator response is corrected for non-linear effects from quenching of the scintillation light and Cherenkov light production. The systematic variation of the

TABLE I: Estimated systematic uncertainties relevant for the neutrino oscillation parameters  $\Delta m_{21}^2$  and  $\theta_{12}$ . The total uncertainty on  $\Delta m_{21}^2$  is 2.0%, while the total uncertainty on the expected event rate (and mainly affecting  $\theta_{12}$ ) is 4.1%.

|                   | Detector-related (%) | Reactor-related (%) |                            |     |
|-------------------|----------------------|---------------------|----------------------------|-----|
| $\Delta m_{21}^2$ | Energy scale         | 1.9                 | $\bar{\nu}_e$ -spectra [7] | 0.6 |
| Event rate        | Fiducial volume      | 1.8                 | $\bar{\nu}_e$ -spectra     | 2.4 |
|                   | Energy threshold     | 1.5                 | Reactor power              | 2.1 |
|                   | Efficiency           | 0.6                 | Fuel composition           | 1.0 |
|                   | Cross section        | 0.2                 | Long-lived nuclei          | 0.3 |

energy reconstruction over the data-set give an absolute energy scale uncertainty of 1.4%; the distortion of the E-scale results in a 1.9% uncertainty on  $\Delta m_{21}^2$ , while the uncertainty at the analysis threshold gives a 1.5% uncertainty on the event rate. Table I summarizes the systematic uncertainties in determining the neutrino oscillation parameters. The uncertainty on  $\Delta m_{21}^2$  is 2.0%, while the uncertainty on the expected event rate, which primarily affects  $\theta_{12}$ , is 4.1%.

For the analysis we require  $0.9 \text{ MeV} < E_p < 8.5 \text{ MeV}$ . The delayed energy  $E_d$  must satisfy  $1.8 \text{ MeV} < E_d < 2.6 \text{ MeV}$  or  $4.0 \text{ MeV} < E_d < 5.8 \text{ MeV}$ , corresponding to the neutron-capture  $\gamma$  energies for protons and  $^{12}\text{C}$ , respectively. The time difference ( $\Delta T$ ) and distance ( $\Delta R$ ) between the prompt event and delayed neutron capture are selected to be  $0.5 \mu\text{s} < \Delta T < 1000 \mu\text{s}$  and  $\Delta R < 2 \text{ m}$ . The accidental coincidence rate rapidly increases near the balloon surface ( $R = 6.5 \text{ m}$ ), reducing the signal-to-background ratio. We use constraints on event characteristics to suppress accidental backgrounds while maintaining high efficiency. The prompt and delayed radial distance from the detector center ( $R_p, R_d$ ) must be less than 6 m. To discriminate signal from background, we construct a probability density function (PDF) for accidental coincidence events,  $f_{acc}(E_d, \Delta R, \Delta T, R_p, R_d)$ , by pairing events in a delayed-coincidence window between 10 ms and 20 s. A PDF for the  $\bar{\nu}_e$  signal,  $f_{\bar{\nu}_e}(E_d, \Delta R, \Delta T, R_p, R_d)$ , is created by a Monte Carlo simulation of the prompt and delayed events using the measured neutron capture time ( $207.5 \pm 2.8 \mu\text{s}$ ) and detector energy resolution. In determining  $f_{\bar{\nu}_e}$ , we integrate  $E_p$  over the oscillation-free reactor spectrum including a contribution from geo-neutrinos estimated from a geological reference model [8]. A discriminator value,  $L = \frac{f_{\bar{\nu}_e}}{f_{\bar{\nu}_e} + f_{acc}}$ , is calculated for each candidate pair that passes the earlier cuts. To discriminate  $\bar{\nu}_e$ -candidates from accidental-background we establish a selection value  $L_{cut}(E_p)$  in prompt energy intervals of 0.1 MeV optimized for maximal signal sensitivity ( $L > L_{cut}(E_p)$  for signal-like events).  $L_{cut}(E_p)$  is the value of  $L$  at which the figure-of-merit,  $\frac{S}{\sqrt{S+B_{acc}}}$  is maximal, where  $S$  and  $B_{acc}$  are the number of signal and accidental-background events calculated from  $f_{\bar{\nu}_e}$  and  $f_{acc}$ , respectively.

The selection efficiency  $\epsilon(E_p)$  is estimated from the fraction of selected coincidence events relative to the total generated in  $R < 6 \text{ m}$  in the simulation, see Fig. 1(top). The increas-

TABLE II: Estimated backgrounds after selection efficiencies.

| Background  | Contribution     |
|---|------------------|
| Accidentals   | $80.5 \pm 0.1$   |
| ${}^9\text{Li}/{}^8\text{He}$   | $13.6 \pm 1.0$   |
| Fast neutron & Atmospheric $\nu$  | $<9.0$           |
| ${}^{13}\text{C}(\alpha,n){}^{16}\text{O}$ G.S.   | $157.2 \pm 17.3$ |
| ${}^{13}\text{C}(\alpha,n){}^{16}\text{O}$ ${}^{12}\text{C}(n,\gamma){}^{12}\text{C}$ (4.4 MeV $\gamma$ ) | $6.1 \pm 0.7$    |
| ${}^{13}\text{C}(\alpha,n){}^{16}\text{O}$ 1 <sup>st</sup> exc. state (6.05 MeV $e^+e^-$ )                | $15.2 \pm 3.5$   |
| ${}^{13}\text{C}(\alpha,n){}^{16}\text{O}$ 2 <sup>nd</sup> exc. state (6.13 MeV $\gamma$ )                | $3.5 \pm 0.2$    |
| Total   | $276.1 \pm 23.5$ |

ing accidental rate at low energies results in a lower efficiency. Above the  ${}^{208}\text{Tl}$  Compton shoulder at 2.6 MeV,  $\epsilon$  reaches 93% reflecting the efficiency of spatial and temporal cuts ( $R_p$ ,  $R_d$ ,  $\Delta R$ ,  $\Delta T$ ) alone. The systematic uncertainty in  $\epsilon$  is evaluated using  ${}^{68}\text{Ge}$  and  ${}^{241}\text{Am}{}^9\text{Be}$  deployments to estimate the space correlation uncertainties. The efficiency above 2.6 MeV differs less than 0.5% relative to the efficiency determined from Monte Carlo; in the region below 1.4 MeV it differs by  $\sim 7\%$ . The average efficiency change over the full spectrum is 0.6%.

The dominant background is caused by  ${}^{13}\text{C}(\alpha,n){}^{16}\text{O}$  reactions. The prime  $\alpha$  particle source is the decay of  ${}^{210}\text{Po}$ , a daughter of the  ${}^{222}\text{Rn}$  decay chain introduced into the LS during assembly. From observations of the quenched scintillator signal from the 5.3 MeV  $\alpha$ , we estimate that there are  $(5.56 \pm 0.22) \times 10^9$   ${}^{210}\text{Po}$   $\alpha$ -decays. While the  ${}^{13}\text{C}$  abundance is only 1.1% of the carbon in the LS, the reaction rate is significant, resulting in neutrons with energies up to 7.3 MeV. These neutrons primarily undergo n-p scattering and most of the observed scintillation energy spectrum is quenched below 2.7 MeV. In addition,  ${}^{12}\text{C}(n,\gamma){}^{12}\text{C}$  (4.4 MeV  $\gamma$ ) and the 1<sup>st</sup> (6.05 MeV,  $e^+e^-$ ) and 2<sup>nd</sup> (6.13 MeV  $\gamma$ ) excited states of  ${}^{16}\text{O}$  produce signals in coincidence with the scattered neutron but the exact cross sections are not well known. A  ${}^{210}\text{Po}{}^{13}\text{C}$  source was employed to study the  ${}^{13}\text{C}(\alpha,n){}^{16}\text{O}$  reaction and tune a simulation using the cross sections from Ref. [9, 10]. We find that the cross sections for the excited  ${}^{16}\text{O}$  states from Ref. [9] agree with the  ${}^{210}\text{Po}{}^{13}\text{C}$  data after scaling the 1<sup>st</sup> excited state by 0.6; the 2<sup>nd</sup> excited state requires no scaling. For the ground-state we use the cross section from Ref. [10] after subtracting the scaled excited states while accounting for the energy-dependent neutron detection efficiency [11] and scaling the resulting spectrum by 1.05. Including the  ${}^{210}\text{Po}$  decay-rate, we assign an uncertainty of 11% for the ground-state and 20% for the excited states. Accounting for  $\epsilon(E_p)$ , there should be  $182.0 \pm 21.7$   ${}^{13}\text{C}(\alpha,n){}^{16}\text{O}$  events in the data-set.

To mitigate background arising from the cosmogenic beta delayed-neutron emitters  ${}^9\text{Li}$  and  ${}^8\text{He}$ , we apply a 2 s veto within a 3-m-radius cylinder around the reconstructed tracks of well-identified muons passing through the LS. For muons that either deposit a large amount of energy or cannot be tracked, we apply a 2 s veto of the full detector. We estimate that  $13.6 \pm 1.0$  events from  ${}^9\text{Li}/{}^8\text{He}$  decays remain by fit-

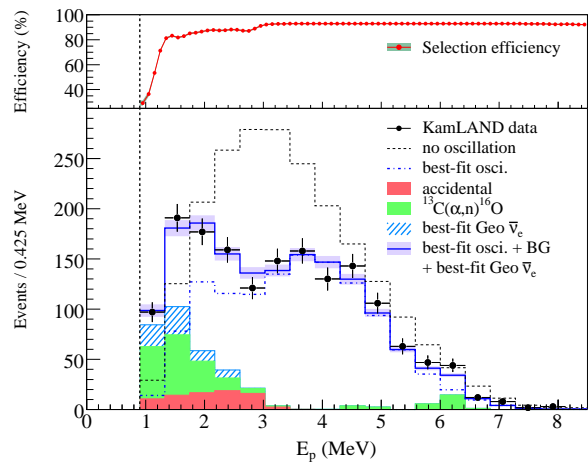


FIG. 1: Prompt event energy spectrum of  $\bar{\nu}_e$  candidate events. All histograms corresponding to reactor spectra and expected backgrounds incorporate the energy-dependent selection efficiency (top panel). The shaded background and geo-neutrino histograms are cumulative. The data show the statistical uncertainties, the band on the blue histogram indicates the event rate systematic uncertainty.

ting the time distribution of identified  ${}^9\text{Li}/{}^8\text{He}$  since the prior muons. Spallation-produced neutrons are suppressed with a 2 ms full-volume veto after a detected muon in the analysis. Some neutrons are produced by muons that are undetected by the OD or miss the OD but interact in the nearby rock. These neutrons can be scattered and then capture in the LS, mimicking the  $\bar{\nu}_e$  signal. We also expect some high-energy background events from atmospheric neutrinos. The energy spectrum of these backgrounds is assumed to be flat to at least 30 MeV based on a simulation following [12]. The atmospheric  $\nu$  spectrum and interactions were modeled using NUANCE [13]. We expect fewer than 9 neutron and atmospheric  $\nu$  events in the data-set. We observe 15 events in the energy range 8.5 MeV to 30 MeV, consistent with the limit reported previously [14].

The accidental coincidence background above 0.9 MeV is measured with a 10-ms-to-20-s delayed-coincidence window to be  $80.5 \pm 0.1$  events. Other backgrounds from  $(\gamma,n)$  interactions and spontaneous fission are negligible.

Anti-neutrinos produced in the decay chains of  ${}^{232}\text{Th}$  and  ${}^{238}\text{U}$  in the Earth's interior are limited to prompt energies below 2.6 MeV. The expected geo-neutrino flux at the KamLAND location is estimated from a reference model [8], which assumes a radiogenic heat production rate of 16 TW from the U and Th-decay chains. The calculated  $\bar{\nu}_e$  fluxes for U and Th-decay, including a suppression factor of 0.57 due to neutrino oscillation, are  $2.24 \times 10^6 \text{ cm}^{-2} \text{ s}^{-1}$  (56.6 events) and  $1.90 \times 10^6 \text{ cm}^{-2} \text{ s}^{-1}$  (13.1 events), respectively.

In the absence of  $\bar{\nu}_e$  disappearance, we expect to observe  $2179 \pm 89$  (syst) events from reactors. The backgrounds in the reactor energy region listed in Table II sum to  $276.1 \pm 23.5$ ; we also expect geo-neutrinos. We observe 1609 events.

Figure 1 shows the prompt energy spectrum of selected electron anti-neutrino events and the fitted backgrounds. The

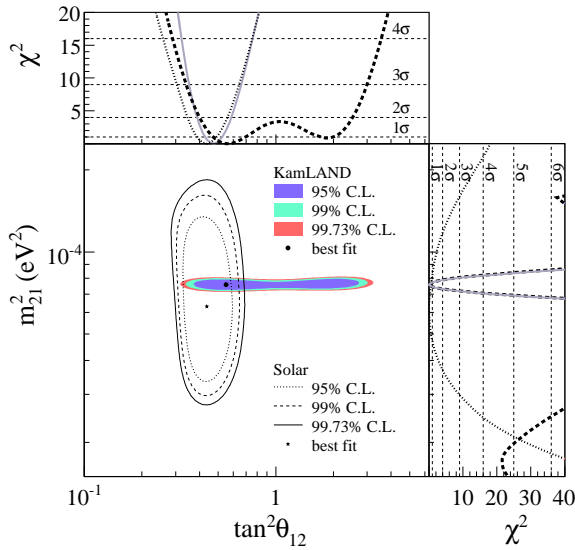


FIG. 2: Allowed region for neutrino oscillation parameters from KamLAND and solar neutrino experiments. The side-panels show the  $\Delta\chi^2$ -profiles for KamLAND (dashed) and solar experiments (dotted) individually, as well as the combination of the two (solid).

unbinned data is assessed with a maximum likelihood fit to two-flavor neutrino oscillation (with  $\theta_{13} = 0$ ), simultaneously fitting the geo-neutrino contribution. The method incorporates the absolute time of the event to account for time variations in the reactor flux and includes Earth-matter oscillation effects. The best-fit is shown in Fig. 1. The joint confidence intervals give  $\Delta m_{21}^2 = 7.58^{+0.14}_{-0.13}(\text{stat})^{+0.15}_{-0.15}(\text{syst}) \times 10^{-5} \text{ eV}^2$  and  $\tan^2 \theta_{12} = 0.56^{+0.10}_{-0.07}(\text{stat})^{+0.10}_{-0.06}(\text{syst})$  for  $\tan^2 \theta_{12} < 1$ . A scaled reactor spectrum without distortions from neutrino oscillation is excluded at more than  $5\sigma$ . An independent analysis using cuts similar to Ref. [2] finds  $\Delta m_{21}^2 = 7.66^{+0.22}_{-0.20} \times 10^{-5} \text{ eV}^2$  and  $\tan^2 \theta_{12} = 0.52^{+0.16}_{-0.10}$ .

The allowed contours in the neutrino oscillation parameter space, including  $\Delta\chi^2$ -profiles, are shown in Fig. 2. Only the so-called LMA-I region remains, while other regions previously allowed by KamLAND at  $\sim 2.2\sigma$  are disfavored at more than  $4\sigma$ . When considering three-neutrino oscillation, the KamLAND data give the same result for  $\Delta m_{21}^2$ , and a slightly increased uncertainty on  $\theta_{12}$ . The parameter space can be further constrained by incorporating the results of SNO [15] and solar flux experiments [16] in a two-neutrino analysis with KamLAND assuming CPT invariance. The oscillation parameters from this combined analysis are  $\Delta m_{21}^2 = 7.59^{+0.21}_{-0.21} \times 10^{-5} \text{ eV}^2$  and  $\tan^2 \theta_{12} = 0.47^{+0.06}_{-0.05}$ .

In order to assess the number of geo-neutrinos, we fit the normalization of the  $\bar{\nu}_e$  energy spectrum from the U and Th-decay chains simultaneously with the neutrino oscillation parameter estimation using the KamLAND and solar data; see Fig. 3. The time of the event gives additional discrimination power since the reactor contribution varies. The fit yields 25 and 36 detected geo-neutrino events from the U and Th-decay chains, respectively, but there is a strong anti-correlation. Fix-

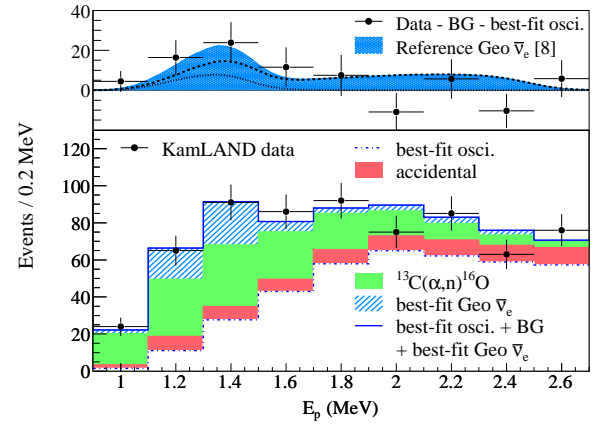


FIG. 3: The low-energy region of the  $\bar{\nu}_e$  spectrum relevant for geo-neutrinos. The main panel shows the data with the fitted background and geo-neutrino contributions; the upper panel compares the background and reactor- $\bar{\nu}_e$ -subtracted data to the number of geo-neutrinos for the decay chains of U (dashed) and Th (dotted) calculated from a geological reference model [8].

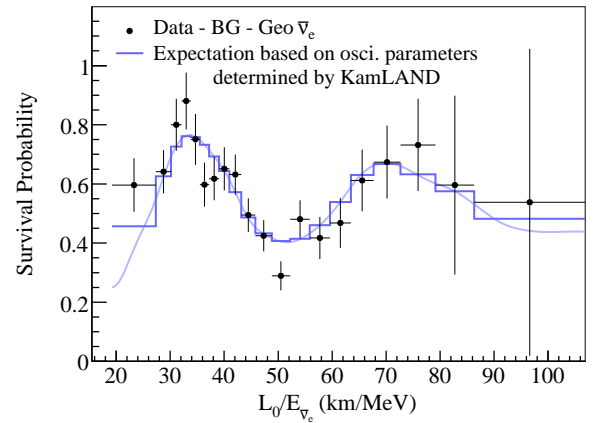


FIG. 4: Ratio of the background and geo-neutrino subtracted  $\bar{\nu}_e$  spectrum to the expectation for no-oscillation as a function of  $L_0/E$ .  $L_0$  is the effective baseline taken as a flux-weighted average ( $L_0 = 180 \text{ km}$ ); the energy bins are equal probability bins of the best-fit including all backgrounds (see Fig. 1). The histogram and curve show the expectation accounting for the distances to the individual reactors, time-dependent flux variations and efficiencies. The error bars are statistical and do not include correlated systematic uncertainties in the energy scale.

ing the Th/U mass ratio to 3.9 from planetary data [17], we obtain a combined U+Th best-fit value of  $73 \pm 27$  events corresponding to a flux of  $(4.4 \pm 1.6) \times 10^6 \text{ cm}^{-2} \text{ s}^{-1}$ , in agreement with the geological reference model.

The KamLAND data, together with the solar  $\nu$  data, set an upper limit of 6.2 TW (90% C.L.) for a  $\bar{\nu}_e$  reactor source at the Earth's center [18], assuming that the reactor produces a spectrum identical to that of a slow neutron artificial reactor.

The ratio of the background-subtracted  $\bar{\nu}_e$  candidate events, including the subtraction of geo-neutrinos, to the expectation assuming no neutrino oscillation is plotted in Fig. 4 as a function of  $L_0/E$ . The spectrum indicates almost two cycles of the

periodic feature expected from neutrino oscillation.

The data presented in this Letter decisively confirm neutrino oscillation, providing the most precise value of  $\Delta m_{21}^2$  to date. KamLAND improves the precision of the value of  $\tan^2 \theta_{12}$  when combined with the solar  $\nu$  data. There continues to be an indication of an excess of low-energy anti-neutrinos consistent with an interpretation as geo-neutrinos.

The KamLAND experiment is supported by the Japanese Ministry of Education, Culture, Sports, Science and Technology, and under the United States Department of Energy Office grant DEFG03-00ER41138 and other DOE grants to individual institutions. The reactor data are provided by courtesy of the following electric associations in Japan: Hokkaido, Tohoku, Tokyo, Hokuriku, Chubu, Kansai, Chugoku, Shikoku and Kyushu Electric Power Companies, Japan Atomic Power Co. and Japan Nuclear Cycle Development Institute. The Kamioka Mining and Smelting Company has provided service for activities in the mine.

---

\* Present address: Center of Quantum Universe, Okayama University, Okayama 700-8530, Japan

† Present address: Department of Physics, Regis University, Denver, Colorado 80221, USA

‡ Present address: FNAL, Batavia, Illinois 60510, USA

§ Present address: SNOLAB, Lively, ON P3Y 1M3, Canada

¶ Present address: LLNL, Livermore, California 94550, USA

- [1] K. Eguchi *et al.* [KamLAND Coll.], Phys. Rev. Lett. **90**, 021802 (2003).
- [2] T. Araki *et al.* [KamLAND Coll.], Phys. Rev. Lett. **94**, 081801 (2005).
- [3] T. Araki *et al.* [KamLAND Coll.], Nature **436**, 499 (2005).
- [4] K. Nakajima *et al.*, Nucl. Instrum. Meth. A **569**, 837 (2006).
- [5] V. I. Kopeikin, L. A. Mikaelyan and V. V. Sinev, Phys. Atom. Nucl. **64**, 849 (2001) [Yad. Fiz. **64**, 914 (2001)].
- [6]  $^{235}\text{U}$  : K. Schreckenbach *et al.*, Phys. Lett. B **160**, 325 (1985);  $^{239,241}\text{Pu}$  : A. A. Hahn *et al.*, Phys. Lett. B **218**, 365 (1989);  $^{238}\text{U}$  : P. Vogel *et al.*, Phys. Rev. C **24**, 1543 (1981).
- [7] B. Achkar *et al.*, Phys. Lett. B **374**, 243 (1996).
- [8] S. Enomoto *et al.*, Earth Planet. Sci. Lett. **258**, 147 (2007).
- [9] JENDL, the Japanese Evaluated Nuclear Data Library available at <http://www.ndc.tokai-sc.jaea.go.jp/jendl/jendl.html> (2005).
- [10] S. Harissopoulos *et al.*, Phys. Rev. C **72**, 062801 (2005).
- [11] H. W. Becker, private communication.
- [12] M. G. Marino *et al.*, Nucl. Instrum. Meth. A **582**, 611 (2007).
- [13] D. Casper, Nucl. Phys. Proc. Suppl. **112**, 161 (2002).
- [14] K. Eguchi *et al.* [KamLAND Coll.], Phys. Rev. Lett. **92**, 071301 (2004).
- [15] B. Aharmim *et al.* [SNO Coll.], Phys. Rev. C **72**, 055502 (2005).
- [16] J. N. Bahcall, A. M. Serenelli and S. Basu, Astrophys. J. **621**, L85 (2005).
- [17] A. Rocholl and K. P. Jochum, Earth Planet. Sci. Lett. **117**, 265 (1993).
- [18] J. M. Herndon, Proc. Nat. Acad. Sci. **100**, 3047 (2003).
- [19] Previous publications incorrectly indicated 1.52 g/l of PPO.